Dynamical phase transition in the open Dicke model

Jens Klinder, Hans Keßler, Matthias Wolke, Ludwig Mathey, and Andreas Hemmerich[1]

Institut für Laser-Physik, Universität Hamburg, 22761 Hamburg, Germany

Edited by Peter Zoller, University of Innsbruck, Innsbruck, Austria, and approved January 15, 2015 (received for review September 4, 2014)

The Dicke model with a weak dissipation channel is realized by coupling a Bose–Einstein condensate to an optical cavity with ultranarrow bandwidth. We explore the dynamical critical properties of the Hepp–Lieb–Dicke phase transition by performing quenches across the phase boundary. We observe hysteresis in the transition between a homogeneous phase and a self-organized collective phase with an enclosed loop area showing power-law scaling with respect to the quench time, which suggests an interpretation within a general framework introduced by Kibble and Zurek. The observed hysteretic dynamics is well reproduced by numerically solving the mean-field equation derived from a generalized Dicke Hamiltonian. Our work promotes the understanding of nonequilibrium physics in open many-body systems with infinite range interactions.

dynamical phase transition | critical behavior | Dicke model | quantum gas | cavity QED

Although equilibrium phases in quantum many-body systems have been explored for a long time with great success, nonequilibrium phenomena in such systems are far less well understood (1). A paradigm for exploring nonequilibrium dynamics is the quench scenario, where a system parameter is subjected to a sudden change between two values associated with different equilibrium phases. Quantum degenerate atomic gases with their unique degree of control are particularly adapted for experimental quench studies (2, 3). For isolated quantum many-body systems a wealth of theoretical and experimental investigations of quench dynamics has appeared recently (4–11). A natural extension of such studies is to consider driven open systems, where dynamical equilibrium states can arise via a competition between dissipation and driving, and nonequilibrium transitions between such phases can occur as a function of some external control parameter (12–15). A nearly ideal experimental platform for this endeavor are quantum degenerate atomic gases subjected to optical high-finesse cavities, where the usual extensive control in cold gas systems can be combined with a precisely engineered coupling to the external bath of vacuum radiation modes (16).

Here, we study a dynamical phase transition in the open Dicke model emulated in an atom–cavity system prepared near zero temperature. The Dicke model is a paradigmatic scenario of quantum many-body physics, still subject to intensive research despite a history more than half a century long (17–28). It describes the interaction of N two-level atoms with a common mode of the electromagnetic radiation field. Hepp and Lieb already pointed out in the 1970s that upon varying the coupling strength, this model possesses a second-order equilibrium quantum phase transition between a homogeneous phase, in which each atom interacts separately with the radiation mode, and a collective phase in which all atomic dipoles align to form a macroscopic dipole moment (19, 22). It has been early suspected that the critical properties of the externally pumped open Dicke model should give rise to nonlinear hysteretic behavior in dynamical experiments (20, 21). The dynamical properties of the open Dicke model and of related many-body atom–cavity systems in the presence of dissipation are subject of extensive recent theoretical research (24, 25, 28–31).

With the atomic levels chosen to be momentum states of the external motion, the open Dicke model has been recently implemented experimentally by coupling a Bose–Einstein condensate (BEC) to a high-finesse resonator pumped by an external optical standing wave (32). A transition from a homogeneous phase (consisting of the condensate with no photons in the cavity) into a collective phase (with the atoms forming a density grating trapped in a stationary intracavity optical standing wave) was observed at a critical pump strength close to the expected equilibrium transition boundary. A related transition with thermal atoms has been studied in earlier work (33, 34). In the formation of the collective phase the Z_2 symmetry, associated with two possible grating configurations shifted with respect to each other by half an optical wavelength, is spontaneously broken (34, 35). In ref. 32 the cavity dissipation rate was more than two orders of magnitude larger than the single-photon recoil frequency with the consequences that the intracavity light field adiabatically adjusts to the evolution of the atomic distribution on a microsecond time scale.

In the present work, the main innovation is the use of a cavity with ultranarrow bandwidth on the order of the single-photon recoil frequency (36, 37). The time scales for dissipation of the intracavity field and the coherent atomic evolution are similar. We can thus dynamically access the nonadiabatic regime, where both quantities are not in equilibrium and hence explore nonequilibrium critical properties of the Dicke model in quench experiments. For different signs of the effective detuning δ_{eff} of the pump field with respect to the cavity resonance, we observe fundamentally different behavior. Remarkably, the Hepp–Lieb–Dicke transition, observed for negative detuning $\delta_{\mathrm{eff}} < 0$, shows a dynamical hysteresis. The resulting hysteresis loop encloses an area which exhibits power-law dependence upon the duration of the quench across the phase boundary and maintains nonzero values even at quench time scales far slower than the dynamical time scales of the underlying single-particle Hamiltonian. We interpret this finding in the framework of the Kibble–Zurek model (38–40). Our observations are consistent with solutions of the mean-field equations associated with a Dicke Hamiltonian

Significance

Nonequilibrium phenomena in quantum many-body systems are not well understood to date. This applies in particular for open systems, coupled to an external bath. We use a Bose–Einstein condensate in a high-finesse optical resonator with ultralow bandwidth to emulate the open Dicke model. In well-controlled sweeps across the Hepp–Lieb–Dicke phase transition, we observe hysteretic dynamics showing power-law scaling with respect to the transition time, which suggests an interpretation in terms of a Kibble–Zurek mechanism. Our observations indicate the possibility of universal behavior in the presence of dissipation.

Author contributions: A.H. designed research; J.K., H.K., and M.W. performed research; L.M. and A.H. contributed new reagents/analytic tools; J.K., H.K., M.W., and A.H. analyzed data; and A.H. wrote the paper.

The authors declare no conflict of interest.

This article is a PNAS Direct Submission.

Freely available online through the PNAS open access option.

[1]To whom correspondence should be addressed. Email: hemmerich@physnet.uni-hamburg.de.

This article contains supporting information online at www.pnas.org/lookup/suppl/doi:10.1073/pnas.1417132112/-/DCSupplemental.

(17). A second interesting consequence is the observation of an instability boundary for positive detuning $\delta_{\rm eff} > 0$. The physics of this instability, which is also predicted by the Dicke model but not much discussed in the literature, resembles cavity-assisted matter wave superradiance (41), recently observed to prevail at any value of $\delta_{\rm eff}$ for single-sided pumping (42). The system is excited by a cascade of successive superradiant pulses to form coherent superpositions of discrete momentum states with the zero momentum condensate mode practically depleted. No stationary intracavity field is formed in this case. At the boundary between the two regimes within a narrow interval around zero detuning $\delta_{\rm eff} \approx 0$ we find that the atoms cannot scatter photons at all even at large values of the pump strength.

Experimental Scheme

In our experiment, outlined in Fig. 1*A*, a cigar-shaped BEC of ^{87}Rb-atoms is prepared such that its long axis is well aligned with the axis of a longitudinal mode of a high-finesse ($\mathcal{F} = 3.44 \pm 0.05 \times 10^5$) optical standing wave resonator. The atoms are exposed to an optical standing wave oriented perpendicularly with respect to the cavity axis. The strength of this external pump wave is parametrized by the depth ε_p of the associated light shift potential in units of the recoil energy, which is determined spectroscopically (for details see *SI Appendix*). The frequency ω_p of the pump wave is far detuned from the relevant atomic resonances, such that the interaction with the atoms is dispersive with negligible spontaneous emission (for details see *SI Appendix*). The cavity possesses an extremely low dissipation rate associated with the loss of photons. The field decay rate $\kappa = 2\pi \times 4.45 \pm 0.05$ kHz is smaller than twice the recoil frequency $2\,\omega_{\rm rec} = 2\pi \times 7.1$ kHz, which corresponds to the kinetic energy transferred to a resting atom by scattering a pump photon into the cavity and hence sets the time scale of the atomic motion. As a consequence, the choice of ω_p relative to the resonance frequency ω_c of the empty cavity selects only a small fraction of the atomic momentum states, illustrated in Fig. 1*B*, to be resonantly coupled. For a uniform atomic sample and left circularly polarized light, the TEM_{00} resonance frequency is dispersively shifted by an amount $\delta_- = (1/2)N_a\,\Delta_-$ with an experimentally determined light shift per photon $\Delta_- \approx 2\pi \times 0.36 \pm 0.04$ Hz. With $N_a = 10^5$ atoms $\delta_- = 2\pi \times 18$ kHz, which amounts to 4 κ, i.e., the cavity operates well within the regime of strong cooperative coupling (for details see *SI Appendix*).

Hepp–Lieb–Dicke Transition

For negative detuning $\delta_{\rm eff} \equiv \omega_p - \omega_c - \delta_- < 0$, above a critical value of ε_p, a stationary intracavity light field builds up and the atoms are captured in the ground state of the light shift potential formed by the interference of the intracavity field and the pump wave. In Fig. 2*A*, the observed intracavity power is plotted versus $\delta_{\rm eff}$ and ε_p. This graph is obtained by linearly ramping up ε_p at a rate $1.4\,E_{\rm rec}$ ms^{-1} at fixed values of $\delta_{\rm eff}$. The formation of the optical lattice is readily seen by detecting Bragg maxima in the atomic momentum spectra obtained by a time-of-flight method. In Fig. 2*B* this is shown for the position in the phase diagram in Fig. 2*A* marked by the white cross. Within a narrow channel around $\delta_{\rm eff} = 0$, scattering of photons is entirely suppressed. Above $\varepsilon_p \approx 5$ this channel becomes so narrow that our limited accuracy of the pump frequency (about $\pm$ 200 Hz) does not provide sufficient resolution. This may be understood as follows: For $|\delta_{\rm eff}|$ exceeding κ, the intracavity field is driven in phase with the pump field. Hence, interference of the two fields yields a square lattice potential with minima arranged on a Bravais lattice spanned by the primitive vectors $(\hat{y} \pm \hat{z})\lambda_p/2$ with $\hat{y}$, $\hat{z}$ denoting the unit vectors in y- and z directions, respectively. The density grating formed by trapping atoms in these minima (corresponding to the intensity maxima in Fig. 1*A*) satisfies the Bragg condition for scattering photons from the pump field into the cavity. When $|\delta_{\rm eff}|$ becomes smaller than κ, the relative phase between the intracavity field and the pump field approaches $\pi/2$ for $|\delta_{\rm eff}| \to 0$. This suppresses the interference between both fields. As a result, the unit cell develops a second minimum, which approaches equal depth for $\delta_{\rm eff} \to 0$. The associated density grating, now populating both classes of minima, no longer supports Bragg scattering of pump photons into the cavity, and hence the intracavity field and the density grating collapse.

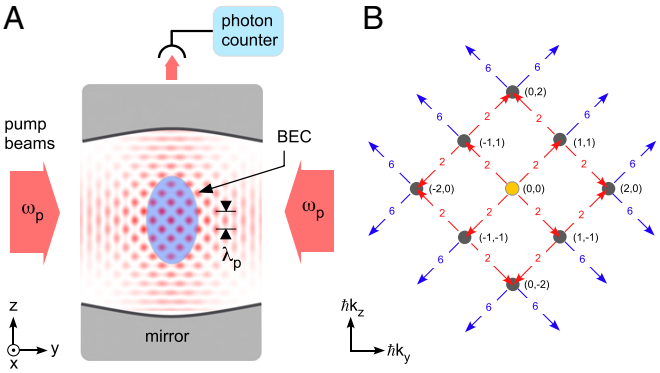

Fig. 1. (*A*) Experimental scheme. The intracavity intensity is indicated by the red pattern with the antinodes corresponding to the locations where the atoms are localized. The frequency and wavelength of the pump beams are denoted by ω_p and λ_p, respectively. (*B*) The available atomic momentum states that can couple to the condensate are indicated by their momentum components (n, m) in the y- and z directions in units of the pump photon momentum $\hbar k$. Arrows of the same color identify scattering processes involving the same kinetic energy transfer, denoted in units of the recoil energy $E_{\rm rec} \equiv \hbar\omega_{\rm rec} \equiv \hbar^2 k^2/2m$ (m = atomic mass) by the numbers on top of the arrows.

The basic structure of the observations in Fig. 2*A* can be understood as follows. At low pump powers the dynamics of the system may be described by the Heisenberg equations for the matter and light variables associated with the Dicke Hamiltonian with an additional term describing dissipation of the cavity light field at a rate κ (for details see *SI Appendix*). These equations possess a stationary solution describing the homogeneous phase, when all atoms populate the condensate mode at zero intracavity intensity. Linearization around this solution yields a stability matrix, whose eigenvalues are readily calculated. Their real parts denote the excitation spectrum whereas their imaginary parts denote the corresponding exponential excitation rates. Hence, if one of the eigenvalues attains a positive imaginary part, the homogeneous phase becomes unstable. The maximum of the imaginary parts of all eigenvalues, denoted by $\gamma_{\rm exc}$, is plotted in Fig. 2*C* versus $\delta_{\rm eff}$ and ε_p. Fig. 2 *D* and *E* shows the excitation frequencies (blue solid lines) and the corresponding excitation rates (red dashed lines) along vertical sections in Fig. 2*C* with fixed detunings $\delta_{\rm eff} = \pm 2\pi \times 20$ kHz. The solid red lines highlight the maxima $\gamma_{\rm exc}$ of the excitation rates. For negative detuning, below a critical value of ε_p the homogeneous phase is predicted to be stable. As the critical value $\varepsilon_{p,c}$ is approached, a softening of one of the excitation modes is seen in Fig. 2*D* (descending solid blue line starting at $2\,E_{\rm rec}$) and as $\varepsilon_{p,c}$ is passed, $\gamma_{\rm exc}$ attains positive values (solid red line), indicating instability of the homogeneous phase. In Fig. 2*C*, $\varepsilon_{p,c}(\delta_{\rm eff})$ is highlighted by a red dashed line, which indicates the expected equilibrium Dicke phase transition boundary. This boundary is also registered in the data in Fig. 2*A*.

Observation of Hysteresis

As is seen in Fig. 2*A*, the phase transition for increasing ε_p is observed at values of ε_p beyond the equilibrium phase boundary. As also noted in ref. 25, this should be expected because sufficiently

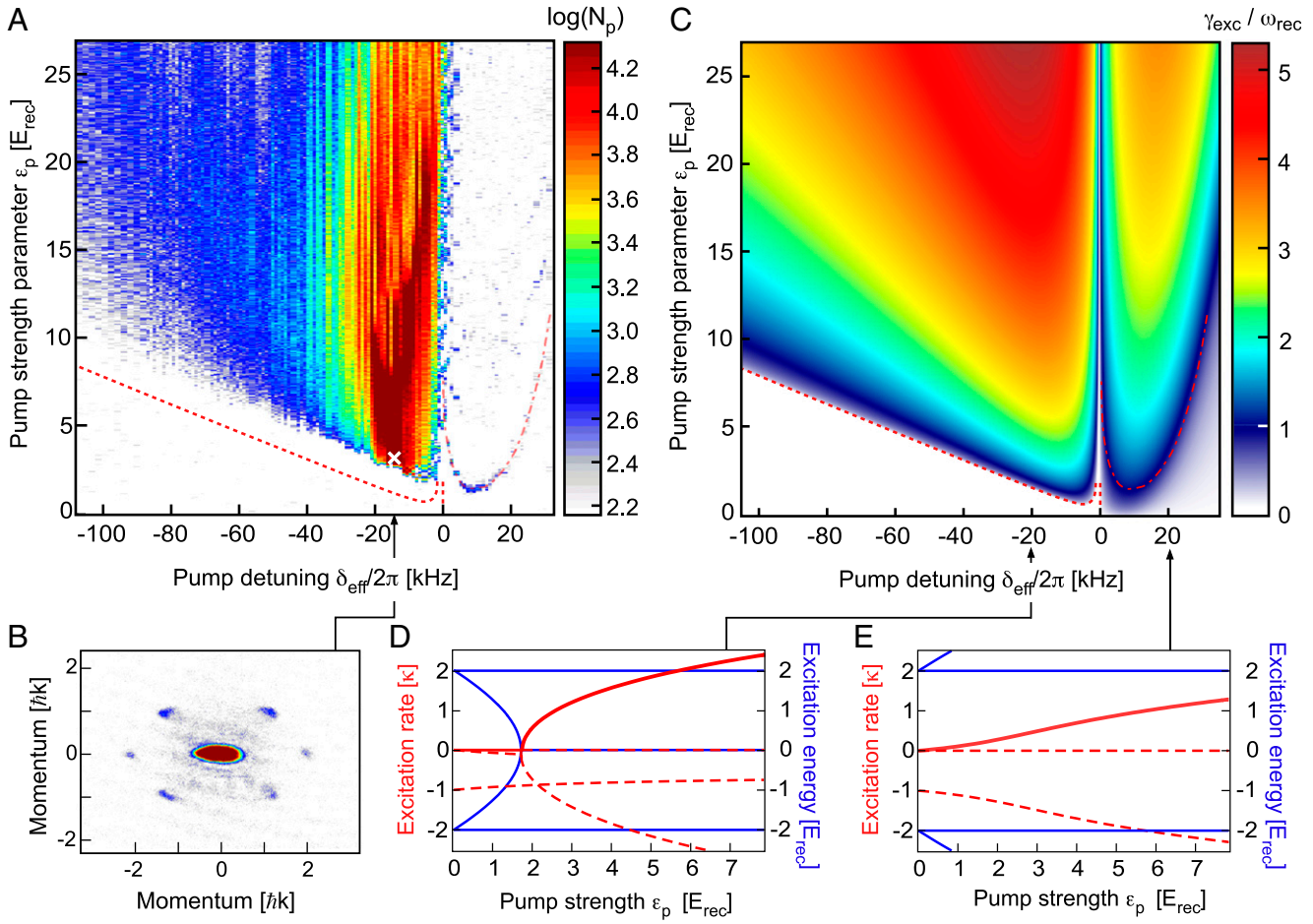

Fig. 2. (*A*) Observed intracavity photon number N_p is plotted versus the pump strength parameter ε_p and the pump detuning δ_{eff}. (*B*) A momentum spectrum is shown recorded at the point in *A* marked by the white cross. The dashed red line indicates the equilibrium Dicke phase boundary obtained from the stability analysis illustrated in *C*. (*C*) Plot of the maximal excitation rate γ_{exc} calculated from a stability analysis for the homogeneous phase of the Dicke model. For negative δ_{eff}, the equilibrium Dicke phase transition line is highlighted by the red dashed line. For positive δ_{eff}, the dashed-dotted red line indicates the contour $\gamma_{\text{exc}} \approx 0.8\ \omega_{\text{rec}}$, where superradiant pulses are observed in *A*. (*D* and *E*) For $\delta_{\text{eff}} = \pm 2\pi \times 20$ kHz the real (solid blue lines) and imaginary (dashed red lines) parts of all eigenvalues of the stability matrix are plotted. The maximal values of the latter are highlighted by the solid red lines.

large values of γ_{exc} must be reached in Fig. 2*C* before the system can leave the homogeneous phase in a given time. A more complete picture is provided in Fig. 3, where the transition through the phase boundary is studied for negative detuning $\delta_{\text{eff}} = -2\pi \times 17.5$ kHz in more detail. In Fig. 3*A* ε_p is ramped up from 0 to 4 in 1.5 ms and back to 0 again in 1.5 ms. The solid blue and red lines show the observed intracavity intensity for the increasing and decreasing sections of the ramp, respectively. Note that this quantity measures the depth of the intracavity lattice emerging in the collective phase and hence corresponds to the square of the order parameter for the Dicke phase transition. A significant hysteresis is observed. For increasing ε_p a sudden jump of the intracavity intensity arises on a time scale corresponding to the cavity decay rate. On the way back, the intracavity intensity is smoothly tuned to zero. In the center row of the figure (below Fig. 3 *A* and *B*), a series of consecutively numbered momentum spectra is shown, recorded at different instances of time during the ε_p-ramp, indicated by the correspondingly numbered arrows in Fig. 3*A*. As the intracavity intensity assumes finite values, a coherent optical lattice is formed (arrow 2), as is seen from the occurrence of higher-order Bragg peaks. As the lattice depth grows (arrows 3 and 4), tunneling amplitudes decrease, and the relatively increased collisional interaction acts to reduce particle number fluctuations resulting in a loss of coherence. When ramping back to small values of ε_p, the BEC is recovered with no notable atom loss and only few low-energy Bogoliubov excitations (arrow 5).

In Fig. 3*B* a mean-field calculation (based upon a Dicke Hamiltonian, *SI Appendix*) is shown for a homogeneous, infinite system without collisional interaction, which shows the same signatures as observed in Fig. 3*A* including dynamical details as the oscillation of the red trace around $\varepsilon_p \approx 2.5$ and the overshooting of the blue trace around $\varepsilon_p \approx 3.5$. The observed hysteresis appears fundamentally different from that known to occur in conventional bistable systems, where discontinuities arise for both critical values, where the system becomes unstable. We do not find a discontinuity at the lower critical value $\varepsilon_{p,1}$ in Fig. 3 *A* and *B*; however, the system always follows the blue curve, when this point is passed with increasing ε_p, irrespective of the duration τ_Q of the applied ε_p-ramp. For increasing cavity bandwidths our mean-field calculations predict that the area enclosed by the hysteresis decreases and finally is obscured by increasing optomechanical oscillations at the phase boundary (see also figure 12a in ref. 25).

Power-Law Scaling

The dependence of the threshold values $\varepsilon_{p,1}$ and $\varepsilon_{p,2}$ for the dynamical transitions in Fig. 3 *A* and *B* upon the quench time τ_Q

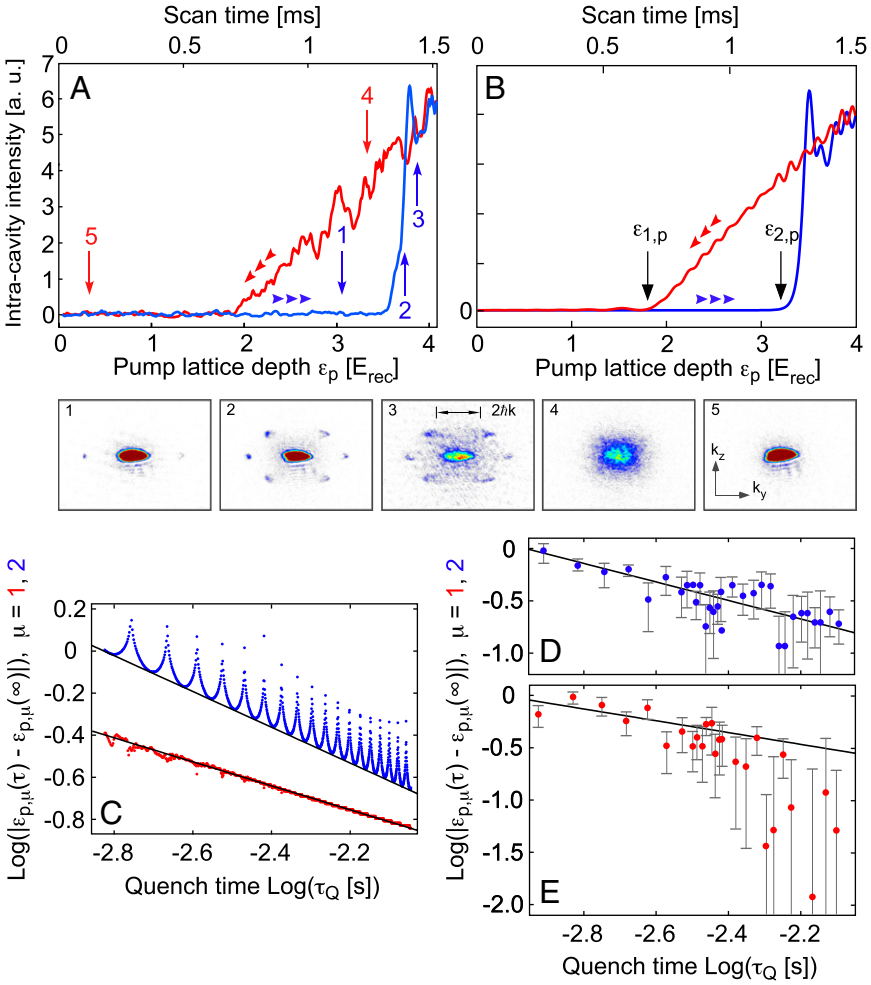

Fig. 3. (*A*) For fixed $\delta_{\text{eff}} = -2\pi \times 17.5$ kHz the intracavity intensity is plotted with the pump strength ramped from 0 to 4 E_{rec} in 1.5 ms (blue line) and back (red line). Below *A*, a series of consecutively numbered momentum spectra is shown (1–5), recorded at increasing times during the ε_p-ramp, indicated by the correspondingly numbered arrows in *A*. (*B*) Mean-field calculation according to *A* for a homogeneous, infinite system without collisional interaction. (*C*) Mean-field calculations of $\varepsilon_{p,1}$ (*Lower*, red dots) and $\varepsilon_{p,2}$ (*Upper*, blue dots) are shown. The solid lines show power laws with exponents $n_1 = -0.57$ (*Lower*) and $n_2 = -0.85$ (*Upper*). The measured dependence of the critical values $\varepsilon_{p,\mu}, \mu \in \{1,2\}$ upon the quench time τ_Q is shown for $\mu = 2$ in *D* and for $\mu = 1$ in *E*. The solid lines repeat the power laws found in the mean-field calculations in *C*. The error bars reflect the SDs for 10 measurements.

is studied in Fig. 3 *C*–*E*. These quantities are determined as those values of ε_p where the intracavity intensity assumes 5% of its maximal value reached for $\varepsilon_p = 4$. In Fig. 3*C* the values of $\Delta\varepsilon_{p,\mu}(\tau_Q) \equiv \varepsilon_{p,\mu}(\tau_Q) - \varepsilon_{p,\mu}(\tau_Q = \infty)$ $(\mu \in \{1,2\})$, calculated from curves such as that shown in Fig. 3*B*, are plotted versus τ_Q. As shown by the solid lines, the τ_Q-dependences follow power laws $\Delta\varepsilon_{p,\mu}(\tau_Q) \propto \tau_Q^{n_\mu}$ with $n_1 = -0.57$ and $n_2 = -0.85$. The phase offset of the sharp resonances occurring periodically at a frequency $\Omega = 0.682\ \omega_{\text{rec}}$ in the upper blue trace depends on the specific choice of a small initial excitation, necessary to drive the system out of the homogeneous phase, which is provided by quantum and thermal fluctuations in the experiment. The exponents n_1, n_2 turn out independent of the exact initial conditions (for details see *SI Appendix*). In Fig. 3 *D* and *E* we plot the experimentally observed values of $\Delta\varepsilon_{p,\mu}(\tau_Q)$ with $\mu = 2$ and $\mu = 1$, respectively. The solid lines repeat the power laws found in the calculations in Fig. 3*C* with $n_2 = -0.85$ in Fig. 3*D* and $n_1 = -0.57$ in Fig. 3*E*. Whereas in Fig. 3*D* the data nicely agree with the power-law behavior, in Fig. 3*E* this is only the case for the first half of the plot. At later times the data points assume an exponential rather than a power-law decay, which is in accordance with the observation that for long ramp times at the end of the descending ramp notable particle loss sets in. Our observations of power-law behavior of $\Delta\varepsilon_{p,\mu}(\tau_Q)$ suggest an interpretation within the universal model introduced by Kibble and Zurek (38–40), which applies for second-order phase transitions in isolated many-body systems. According to this model a quench between two phases is approximated by a succession of an adiabatic approach toward and a departure from the equilibrium critical point $\varepsilon_{p,c}$ conjoined by a diabatic passage through the critical point, where the dynamics is completely frozen. Furthermore, a power-law dependence for the relaxation time is assumed, i.e., $\tau(\varepsilon_p) \propto \left|\varepsilon_p - \varepsilon_{p,c}\right|^{-z_\mu \nu_\mu}$, with $\mu \in \{1,2\}$ if $\varepsilon_p < \varepsilon_{p,c}$ and $\varepsilon_p > \varepsilon_{p,c}$, respectively. The identification of $\Delta\varepsilon_{p,\mu}$ with the lower and upper bounds of the diabatic region around $\varepsilon_{p,c}$ then leads to the prediction that $z_\mu \nu_\mu = -(1 + (1/n_\mu))$, i.e., in our system: $z_1\nu_1 = 0.75$, $z_2\nu_2 = 0.18$ (for details see *SI Appendix*). A deeper understanding of these values would require a comprehensive extension of the concept of universality to the case of driven open systems (15).

Matter Wave Superradiance

In the $\delta_{\text{eff}} > 0$ region of Fig. 2*A*, matter wave superradiance prevails (41, 42). Short superradiant pulses with a duration on the order of the intracavity photon life time are emitted by the cavity, if ε_p reaches a critical instability boundary, highlighted by a red dashed-dotted line in Fig. 2*A*. The atoms, initially populating

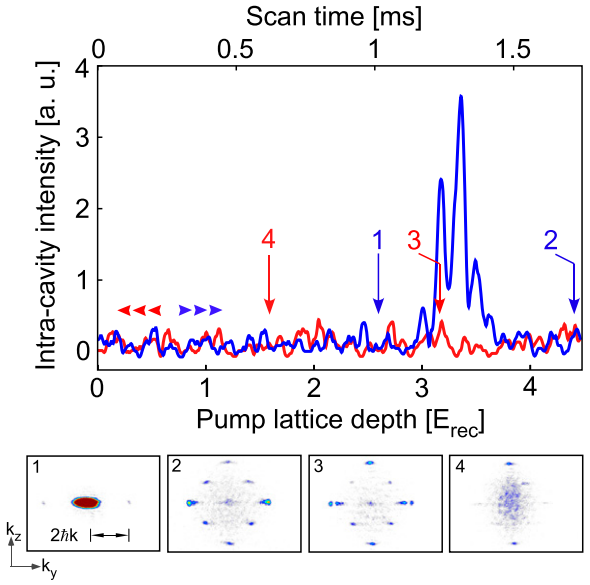

Fig. 4. Intracavity intensity is plotted for fixed detuning $\delta_{\text{eff}} = 2\pi \times 4$ kHz with the pump lattice depth ε_p ramped from 0 to 4.5 E_{rec} in 1.7 ms (blue trace) and back (red trace). At the lower edge of the graph, four numbered momentum spectra are shown, taken at consecutive times, indicated by the numbered arrows.

the condensate mode at zero momentum, are thereby scattered into superpositions of higher momentum states. This excitation is irreversible and cannot be removed by ramping ε_p back to zero. As Fig. 2 *C* and *E* shows, γ_{exc} always exceeds zero for nonzero ε_p. Hence, the homogeneous phase is everywhere unstable. The observed instability boundary corresponds to a contour of constant $\gamma_{\text{exc}} \approx 0.8\ \omega_{\text{rec}}$ (highlighted by the dashed-dotted red line in Fig. 2*C*, replotted from Fig. 2*A*). The value of this constant increases with increasing speed of the applied ε_p-ramp. Our mean-field calculations show that the increase of γ_{exc} with ε_p significantly reduces for increasing cavity bandwidth. Hence, in the experimental scenario of ref. 32, matter wave superradiance is expected to occur only at observation times or values of ε_p much larger than realized there.

Fig. 4 shows the intracavity intensity for fixed positive detuning $\delta_{\text{eff}} = 2\pi \times 4$ kHz with ε_p ramped from 0 to 4.5 E_{rec} in 1.7 ms and back to 0 again in 1.7 ms. At the lower edge of the graph, four numbered momentum spectra are shown, taken at consecutive times, indicated by the numbered arrows. At the chosen value of δ_{eff} the scattering processes indicated by the red arrows in Fig. 1*B*, associated with 2 E_{rec} energy transfer, are nearly resonantly driven, whereas the processes indicated by blue arrows in Fig. 1*B* are significantly detuned, and hence do not contribute. Accordingly, at the threshold value $\varepsilon_p \approx 3\ E_{\text{rec}}$ a short superradiant light pulse is emitted from the cavity, after which a large fraction of the atoms is transferred to the $(\pm 2, 0)\hbar k$ momentum states (arrow 2). These states do not support a matter wave Bragg grating necessary to maintain further scattering. Hence, the cavity field falls to zero and the momentum states propagate toward the trap edges, which are reached in about 1.25 ms corresponding to the trap frequency of 200 Hz in the *y* direction. Reflection of the higher-momentum components at the anharmonic trap edges and collisions yields a rapid broadening of the momentum distribution (arrow 4).

Conclusions

We have studied quench dynamics in the open Dicke model emulated by strongly coupling an atomic BEC to an optical cavity providing an extremely narrow bandwidth. Our experiment exhibits a uniquely controlled paradigm of nonequilibrium many-body dynamics in the presence of dissipation, which appears ideal for quantitative confrontations with theory also beyond mean-field approximations. We hope that this work will stimulate new theoretical efforts to better understand the connection between nonlinear dynamics and statistical mechanics in open many-body systems.

ACKNOWLEDGMENTS. We are grateful to Michael Thorwart, Reza Bakhtiari, Duncan O'Dell, and Helmut Ritsch for useful discussions. This work was partially supported by Deutsche Forschungsgemeinschaft (DFG) under Contracts DFG-SFB 925 and DFG-GrK 1355.

1. Polkovnikov A, Sengupta K, Silva A, Vengalattore M (2011) Non-equilibrium dynamics of closed interacting quantum systems. *Rev Mod Phys* 83(3):863–883.
2. Lewenstein M, et al. (2007) Ultracold atomic gases in optical lattices: Mimicking condensed matter physics and beyond. *Adv Phys* 56(2):243–379.
3. Bloch I, Dalibard J, Zwerger W (2008) Many-body physics with ultracold gases. *Rev Mod Phys* 80(3):885–964.
4. Calabrese P, Cardy J (2006) Time dependence of correlation functions following a quantum quench. *Phys Rev Lett* 96(13):136801.
5. Kollath C, Läuchli AM, Altman E (2007) Quench dynamics and nonequilibrium phase diagram of the Bose-Hubbard model. *Phys Rev Lett* 98(18):180601.
6. Silva A (2008) Statistics of the work done on a quantum critical system by quenching a control parameter. *Phys Rev Lett* 101(12):120603.
7. Heyl M, Polkovnikov A, Kehrein S (2013) Dynamical quantum phase transitions in the transverse-field Ising model. *Phys Rev Lett* 110(13):135704.
8. Sadler LE, Higbie JM, Leslie SR, Vengalattore M, Stamper-Kurn DM (2006) Spontaneous symmetry breaking in a quenched ferromagnetic spinor Bose-Einstein condensate. *Nature* 443(7109):312–315.
9. Kinoshita T, Wenger T, Weiss DS (2006) A quantum Newton's cradle. *Nature* 440(7086):900–903.
10. Gring M, et al. (2012) Relaxation and prethermalization in an isolated quantum system. *Science* 337(6100):1318–1322.
11. Cheneau M, et al. (2012) Light-cone-like spreading of correlations in a quantum many-body system. *Nature* 481(7382):484–487.
12. Hohenberg PC, Halperin BI (1977) Theory of dynamic critical phenomena. *Rev Mod Phys* 43(3):435–479.
13. Diehl S, Tomadin A, Micheli A, Fazio R, Zoller P (2010) Dynamical phase transitions and instabilities in open atomic many-body systems. *Phys Rev Lett* 105(1):015702.
14. Dalla Torre EG, Demler E, Giamarchi T, Altman E (2010) Quantum critical states and phase transitions in the presence of non-equilibrium noise. *Nat Phys* 6:806–810.
15. Sieberer LM, Huber SD, Altman E, Diehl S (2013) Dynamical critical phenomena in driven-dissipative systems. *Phys Rev Lett* 110(19):195301.
16. Ritsch H, Domokos P, Brennecke F, Esslinger T (2013) Cold atoms in cavity-generated dynamical optical potentials. *Rev Mod Phys* 85(2):553–601.
17. Dicke RH (1954) Coherence in spontaneous radiation processes. *Phys Rev* 93(1):99–110.
18. Dicke RH (1964) The coherence brightened laser. *Proceedings of the Third International Congress on Quantum Electronics*, eds Grivet P, Bloembergen N (Columbia Univ Press, New York), pp 35–54.
19. Hepp K, Lieb EH (1973) On the superradiant phase transition for molecules in a quantized radiation field: The Dicke maser model. *Ann Phys* 76:360–404.
20. Gilmore R, Narducci LM (1978) Relation between the equilibrium and nonequilibrium critical properties of the Dicke model. *Phys Rev A* 17(5):1747–1760.
21. Bowden CM, Sung CC (1979) First- and second-order phase transitions in the Dicke model: Relation to optical bistability. *Phys Rev A* 19(6):2392–2401.
22. Gross M, Haroche S (1982) Superradiance: An essay on the theory of collective spontaneous emission. *Phys Rep* 93(5):301–396.
23. Emary C, Brandes T (2003) Quantum chaos triggered by precursors of a quantum phase transition: The Dicke model. *Phys Rev Lett* 90(4):044101.
24. Nagy D, Kónya G, Szirmai G, Domokos P (2010) Dicke-model phase transition in the quantum motion of a Bose-Einstein condensate in an optical cavity. *Phys Rev Lett* 104(13):130401.
25. Bhaseen MJ, Mayoh J, Simons BD, Keeling J (2012) Dynamics of nonequilibrium Dicke models. *Phys Rev A* 85(1):013817.
26. Bastidas VM, Emary C, Regler B, Brandes T (2012) Nonequilibrium quantum phase transitions in the Dicke model. *Phys Rev Lett* 108(4):043003.
27. Piazza F, Strack P, Zwerger W (2013) Bose-Einstein condensation versus Dicke-Hepp-Lieb transition in an optical cavity. *Ann Phys* 339:135–159.
28. Kulkarni M, Öztop B, Türeci HE (2013) Cavity-mediated near-critical dissipative dynamics of a driven condensate. *Phys Rev Lett* 111(22):220408.
29. Gopalakrishnan S, Lev BL, Goldbart PM (2009) Emergent crystallinity and frustration with Bose-Einstein condensates in multimode cavities. *Nat Phys* 5:845–850.
30. Strack P, Sachdev S (2011) Dicke quantum spin glass of atoms and photons. *Phys Rev Lett* 107(27):277202.
31. Dalla Torre EG, Diehl S, Lukin MD, Sachdev S, Strack P (2013) Keldysh approach for nonequilibrium phase transitions in quantum optics: Beyond the Dicke model in optical cavities. *Phys Rev A* 87(2):023831.

32. Baumann K, Guerlin C, Brennecke F, Esslinger T (2010) Dicke quantum phase transition with a superfluid gas in an optical cavity. *Nature* 464(7293):1301–1306.
33. Domokos P, Ritsch H (2002) Collective cooling and self-organization of atoms in a cavity. *Phys Rev Lett* 89(25):253003.
34. Black AT, Chan HW, Vuletić V (2003) Observation of collective friction forces due to spatial self-organization of atoms: From Rayleigh to Bragg scattering. *Phys Rev Lett* 91(20):203001.
35. Baumann K, Mottl R, Brennecke F, Esslinger T (2011) Exploring symmetry breaking at the Dicke quantum phase transition. *Phys Rev Lett* 107(14):140402.
36. Wolke M, Klinner J, Keßler H, Hemmerich A (2012) Cavity cooling below the recoil limit. *Science* 337(6090):75–78.
37. Keßler H, Klinder J, Wolke M, Hemmerich A (2014) Optomechanical atom-cavity interaction in the sub-recoil regime. *New J Phys* 16:053008.
38. Kibble TWB (1976) Topology of cosmic domains and strings. *J Phys A* 9:1387–1398.
39. Zurek WH (1985) Cosmological experiments in superfluid helium? *Nature* 317:505–508.
40. del Campo A, Zurek W (2014) Universality of phase transition dynamics: Topological defects from symmetry breaking. *Int J Mod Phys A* 29:1430018.
41. Inouye S, et al. (1999) Superradiant Rayleigh scattering from a Bose-Einstein condensate. *Science* 285(5427):571–574.
42. Keßler H, Klinder J, Wolke M, Hemmerich A (2014) Steering matter wave superradiance with an ultranarrow-band optical cavity. *Phys Rev Lett* 113(7):070404.